SKB

TECHNICAL REPORT 86-13

Radionuclide transport in fast channels in crystalline rock

Anders Rasmuson, Ivars Neretnieks
Department of Chemical Engineering
Royal Institute of Technology, Stockholm

March 1986

SVENSK KÄRNBRÄNSLEHANTERING AB
SWEDISH NUCLEAR FUEL AND WASTE MANAGEMENT CO

BOX 5864 S-102 48 STOCKHOLM
TEL 08-665 28 00 TELEX 13108-SKB

RADIONUCLIDE TRANSPORT IN FAST CHANNELS IN CRYSTALLINE ROCK

Anders Rasmuson, Ivars Neretnieks

Department of Chemical Engineering
Royal Institute of Technology, Stockholm

March 1985

RADIONUCLIDE TRANSPORT IN FAST CHANNELS IN CRYSTALLINE ROCK

Anders Rasmuson
Ivars Neretnieks

March 1985

Revised February 7, 1986

Department of Chemical Engineering
Royal Institute of Technology
S-100 44 STOCKHOLM
Sweden

In print in Water Resources Research (June 1986)

ABSTRACT

Recent field investigations in crystalline rock give strong indications that water flows in largely isolated channels in fissured rock. The present paper sets out to investigate radionuclide transport in such channels including diffusion into the rock matrix. It is shown that the uptake from a cylindrical hole in a matrix is much more effective, per unit contact area, than a flat surface (semi-infinite solid). Comparison of diffusion from cylindrical and slit-formed channels shows that the differences in interfacial flux are minor. A slit-formed channel may, therefore, be approximated by a cylindrical one. Diffusional transport in the matrix is then treated as 1-D instead of 2-D which gives a considerable numerical simplification. A simple estimate of the "penetration depth" into the cylindrical region, i.e. the location of the diffusional front, is proposed. Using the integrated finite difference method a number of radionuclide transport calculations are performed for the case of flow and dispersion in a cylindrical channel coupled to diffusion and sorption in the matrix.

CONTENTS

BACKGROUND

Water flow in fractured crystalline rock takes place in the fractures or in those parts of the fractures which are open to water flow. Several recent investigations indicate that only a small fraction of the fractures carry water. The larger part of the fractures carry little or no water. The site investigations performed in connection with the Swedish nuclear fuel safety study, KBS-3, during 1978-1983 determined the hydraulic properties of granitic and gneissic rock in six different sites by drilling up to 15 deep (~ 600 m) holes within each site. The holes were mapped for fissures. Hydraulic conductivity measurements were made by two-packer tests with packer intervals ranging from 2 to 25 m, depending on the conductivities.

The hydraulic conductivities were found to lie in the range ~ 10^{-11} m/s (the lower measurement limit) and up to 10^{-7} m/s. Zones with conductivities of up to 10^{-8} m/s have been found even at the larger depths. Although they are not common they seem to occur at intervals on the order of hundred meters. Figure 1 shows the hydraulic conductivity log from Kamlunge (KBS, 1983). Comparisons of the hydraulically conducting zones and the fracture maps from the core logs, have shown that far from all fractures carry water. Figure 2 (KBS, 1983) shows a comparison of the number of visible fractures on the cores at two sites. The frequency of water conducting fractures at both sites is on the order of one in every 5 to 10 meters. The number of visible fractures is 2 to 5 times larger. The water conducting fractures include all fractures where measurable conductivity was obtained. This

means that even the smallest conductivities which are 4 to 5 orders of magnitude smaller than the largest are counted. The smallest fractures will of course carry a very small fraction of the water flow in the rock.

Investigations in the Stripa mine in mid Sweden have shown that the flow in individual fractures takes place in channels (Abelin et al., 1985). Figure 3 shows how the natural water flow emerges from two fractures as they intersect the face of the drift. The white arrows are proportional in length to the flow and the numerical values beside the arrows indicate the magnitude of the flow. Subsequent injection of small amounts of water with nonsorbing tracers (so as not to disturb the natural water flow) showed that significant amounts of the tracers arrived at two of the collection points in the fracture used for the tracer experiment. The collection was made by drilling .5 m long holes in the plane of the fracture with a spacing varying between .5 and .7 m. This means that every hole collected water from about this length of fracture. These results indicate that about 5-20 % of the fracture plane carries more than 90 % of the water. The actual breadth of the channels is less than 1 m and could be considerably smaller.

The tracer residence times and water flow rates have been used to determine the flow porosity (or channel openings) in the channels where the tracer breakthrough curves were obtained. The channel openings were found to be about .1 mm in these channels in one fracture and more than 1 mm in two channels in another fracture. The equivalent fracture openings determined from pressure drop data assuming laminar

flow in a slit (cubic law) give openings on the order of 2-7 micrometers. These results indicate that there are other causes for pressure drop than friction in a smooth slit. The volume of the channel openings is equivalent to that of circular tubes with diameters of 1 to 3 cm.

When the fracture was excavated (5 m times .5 to 1 m) it was found to have fissure coating and rock alteration materials with very varying thickness. Also in some places the rock was more porous than in other and there were instances when the rock broke down to fine "sand" during the coring operations. The injected sorbing tracers were found to be unevenly distributed on the fracture surface. They showed clear indications of channeling. However, the uneven distribution of sorbing tracers is probably also caused by different sorbing capacities of the fracture surface (Abelin et al., 1985).

In another experiment in the Stripa mine a 75 m long drift, with another 25 m long drift intersecting the first drift at right angles, has been excavated. These drifts are also at a depth of 360 m below the ground and natural water level as were the individual fractures. The roof and sides of these drifts have been covered with more than 350 plastic sheets with an area of 2•1 meter. The natural water flow is monitored in these sheets. It has been found that 2/3 of the sheets carry no measurable amount of water flow. One of the sheets obtains about 10 % of the total flow to the tunnel (~ .8 1/hour). 3 % of the sheets get more than half the water flow. The average hydraulic conductivity of the area is between 1 and $10 \cdot 10^{-11}$ m/s. Figure 4 shows the distribution of water flow into the drift (Neretnieks, 1985).

In the program in Switzerland several deep boreholes have been drilled into granitic rock (NAGRA, 1985). In one hole in Böttstein in North eastern Switzerland, very detailed core-mapping and pressure pulse testing in the hole have been performed. It was found that at intervals of less than 100 m there were shear zones (kakeritic) which were strongly altered. The porosity is 3-5 % compared to .5 % for unaltered granite, and some of the quartz has been dissolved. The zones are up to a meter wide. In these zones, quartz-lined holes were found with openings up to a cm in diameter. Their shape varied from round to slit-like openings. The quartz-lining was found to be porous (Skagius, 1985) and would not seriously influence migration by diffusion over the lining. These tubes were deemed to be the major pathways for water flow in the deep lying rock.

A CONCEPT OF WATER FLOW IN FRACTURED CRYSTALLINE ROCK

The above observations together with other visual observations in Stripa and other tunnels in crystalline rock has led us to form an idea of flow in fissured media such as those described which is more based on channeling than on the more often used idea of flow in a (more or less) homogeneous porous medium.

The idea is that the water flows in channels which are quite widely separated and which may not for quite considerable distances intersect other channels. The channels are located in fracture planes and may or may not connect to channels in other fracture planes at fracture intersections. The connected channels may extend for considerable distances before they loose their identity by mixing with other channels.

The individual channels can vary in shape and size; they may be circular tubes at some location and then widen into planar slits with constantly changing widths and openings. The pressure drop is caused by friction in the narrower parts of the conduit and also by fracture filling materials and surface roughness. The flow porosity (channel volume) is not directly related to the pressure drop. Figure 5 shows the main notions of the concepts.

Transport of tracers or radionuclides in such conduits may then be described by the conventional advection-dispersion equation with matrix diffusion effects added. The surface area where flowing water is in contact with the rock surface is much less than if it is assum-

ed that all the surfaces of the rock blocks are actively participating in the exchange. The geometry for the diffusion from a conduit is also quite different from that for diffusion into a block from all sides. In the first case the original contact area is small but the further the migrating species is from the surface the larger the cross section for transport becomes. For the diffusion into blocks, the situation is the opposite.

IMPACT ON RADIONUCLIDE MIGRATION

The migration distances for radionuclides escaping from a repository for high level nuclear waste located in crystalline rock, can be very short if the flow direction is upward. The Swedish study assumes the shortest distance to a major fast pathway to be 100 m. The Swiss repository concept places the repository at 1200 m depth; more than 500 m into the granite underlying the sedimentary rocks. The path length in this case is at least 500 m. In these situations the channels might be assumed not to intersect with other channels to any large degree. This is a conservative assumption as the channels would not mix their waters with each other, evening out the concentrations between fast and slow channels. One would have to investigate the transport properties and the retardation effects of the "worst" channel.

In the analysis below we have chosen the data for the examples based on the following observations and data. The fractures in the rock are spaced at 1 m distance on the average. The fractures are open for .2 m and closed for .8 m on the average. This would give the same information as is shown in Figure 2 where every fifth intersection of the bore hole with the fracture was found to be open, albeit in some cases with very low conductivity. Figure 6 shows how the channels in the fracture planes are arranged in this case. Every channel will have one square meter of rock surrounding it. The channels may or may not have some fracture filling material which has sorbing properties for the nuclides. When the material is sorbing it is assumed that the reaction is reversible and very fast (instantaneous).

MATHEMATICAL MODEL

For flow and sorption from the water in the cylindrical channel we have:

$$R_a \frac{\partial C_f}{\partial t} + V \frac{\partial C_f}{\partial z} - D_L \frac{\partial^2 C_f}{\partial z^2} = - \beta f - R_a \lambda C_f \qquad (1)$$

The terms in this equation represent accumulation in the water in the fissure and on the interface to the solid rock, advective transport, transport by axial dispersion, exchange with the rock matrix, and radioactive decay.

Diffusion and sorption in the cylindrical matrix is given by:

$$K \frac{\partial C_p}{\partial t} = D_p \varepsilon_p \frac{1}{r} \frac{\partial}{\partial r} \left(r \frac{\partial C_p}{\partial r} \right) - K \lambda C_p \qquad (2)$$

In this equation the terms give sorption on the interior surfaces and accumulation in the pore fluid, radial diffusion in the pore fluid, and radioactive decay.

The external surface retardation coefficient R_a is defined as:

$$R_a = 1 + \beta K_f \qquad (3)$$

where K_f is the surface sorption coefficient. The quantity β is the interfacial rock surface per unit channel volume. For a cylindrical matrix it is equal to:

$$\beta = \frac{2}{a} \tag{4}$$

For a nonsorbing species, $R_a = 1$.

K is the volume equilibrium constant and is given by

$$K = \varepsilon_p + K_a \tag{5}$$

where K_a is the intrapore sorption coefficient. For a nonsorbing species, $K = \varepsilon_p$. In general, different linear equilibrium relationships are assumed for the exterior and interior surfaces.

The diffusivity in the water in the micropores, D_p, is related to the diffusivity in pure water, D_v, by

$$D_p = D_v \frac{\delta_D}{\tau^2} \tag{6}$$

where $\delta_D/\tau^2 < 1$ is a geometric factor which accounts for the effects of constrictivity (δ_d) and tortuosity (τ) of the pores in the matrix.

In a system which is initially free of nuclides and in which the inlet ($z = 0$) nuclide concentration is increased to C_0 at time zero the initial and boundary conditions are

$$C_f(0,t) = C_0 e^{-\lambda t} \tag{7}$$

$$C_f(\infty,t) = 0 \tag{8}$$

$$C_f(z,0) = 0 \tag{9}$$

$$C_p(a,z,t) = C_f(z,t) \tag{10}$$

$$C_p(\infty,z,t) = 0 \qquad \text{(11a) (infinite matrix)}$$

$$\frac{\partial C_p}{\partial r}(b,z,t) = 0 \qquad \text{(11b) (finite matrix)}$$

$$C_p(r,z,0) = 0 \tag{12}$$

Boundary condition (10) is the link between (1) and (2).

DIFFUSION FROM CYLINDRICAL CHANNELS

Infinite and finite matrix

In this section we will decouple the flow in the cylindrical channel from the matrix and separately study the matrix diffusion for a non-decaying species into a region bounded internally by a circular cylinder with radius r = a. This case is easier to study but important conclusions may be drawn which have direct bearing on the flow-case. The governing equation (omitting index p) is:

$$K \frac{\partial C}{\partial t} = D_e \frac{1}{r} \frac{\partial}{\partial r} \{r \frac{\partial C}{\partial r}\} \tag{13}$$

We will first study diffusion into an infinite region. The boundary conditions are then:

$$C(a,t) = C_o \tag{14}$$

$$C(\infty,t) = 0 \tag{15}$$

$$C(r,0) = 0 \tag{16}$$

An analytical solution of (13) subject to the boundary conditions (14)-(16) can be found in Carslaw and Jaeger (1959, p. 335). The general solution for the concentration profile $C(r,t)/C_o$ and the flux at the surface $f = - D_e \left.\frac{\partial C}{\partial r}\right|_{r=a}$ as well as approximate solutions valid for small and large times are given in Table 1. The quantity $T = D_a t/a^2$ is a dimensionless time and $\rho = r/a$ is a dimensionless radius.

It is of interest to compare the results for the diffusion from the surface of the region bounded internally by a cylinder with the region bounded internally by a sphere, and the semi-infinite solid. We have:

$$\text{Slab} \quad \frac{C}{C_o} = \operatorname{erfc}\left(\frac{x}{2\sqrt{D_a t}}\right) \qquad (23) \qquad f = \frac{C_o D_e}{\sqrt{\pi D_a t}} \qquad (24)$$

$$\text{Sphere} \quad \frac{C}{C_o} = \frac{a}{r} \operatorname{erfc}\left(\frac{r - a}{2\sqrt{D_a t}}\right) \qquad (25) \qquad f = C_o D_e \left(\frac{1}{\sqrt{\pi D_a t}} + \frac{1}{a}\right) \qquad (26)$$

It is seen that for short times all the profiles and fluxes are identical. This is to be expected since only a thin layer adjacent to the source is affected by the diffusion. In particular the fluxes into a cylindrical and semi-infinite region are the same. For somewhat longer times $f_{cyl} \sim C_o D_e \left(\frac{1}{\sqrt{\pi D_a t}} + \frac{1}{2a}\right)$ which is actually the arithmetic mean of the values for the slab and the sphere. For larger values of T the cylinder flux falls below the mean and as $T \to \infty$ it tends to zero as $2/(a\ell nT)$ while the sphere flux tends to a constant $1/a$. However, for both, the uptake is much more effective than for the slab (with the same interfacial area) where the flux tends to zero as $1/\sqrt{t}$. This is due to the fact that for divergent systems like the cylinder and the sphere a much larger volume is affected at longer times. It should be noted that for large times the diffusional flow into the cylindrical matrix ($\propto af$) is independent of a since $\ell n4T \sim \ell n(4D_a t)$. The fluxes are shown in Figure 7. A further illustration to the difference between diffusion into a semi-infinite solid from a flat surface and a cylindrical region is obtained by noting that the

latter case is analogous to the case of diffusion into a semi-infinite flat solid ($x \geq 0$) with linear increasing diffusivity $D_e = D_{eo}(1+\kappa x)$. If the solid is initially at zero concentration and the surface $x = 0$ is maintained at concentration C_o, the concentration at x at time t is given by the solution in Table 1 for a cylindrical source with:

$$\rho = \sqrt{1 + \kappa x}$$

$$T = \frac{\kappa^2 D_{eo} t}{4K} \tag{27}$$

The flux at the surface $x = 0$ is obtained as:

$$f = - D_{eo} \frac{\partial C}{\partial x}\Big|_{x=0} = \frac{4C_o D_{eo}}{\pi^2} \frac{\kappa}{2} \int_0^\infty \frac{e^{-\lambda^2 T} d\lambda}{\lambda[J_o^2(\lambda) + Y_o^2(\lambda)]} \tag{28}$$

Comparing with the expression for f for the cylindrical source, identity is obtained if $D_{eo} = D_e$ and

$$a = \frac{2}{\kappa} \tag{29}$$

i.e. the fluxes are identical for all times if the radius of the cylindrical source is inversely proportional to the rate of increase of D_e with x. Obviously a small radius a corresponds to a large value of κ again illustrating the effectiveness of a small cylindrical source.

The integrals in the general solutions for the profile and the flux are evaluated by splitting the integral into two parts:

$$\int_0^{\infty} = \int_0^{\alpha} + \int_{\alpha}^{\infty} \tag{30}$$

The first integral (for small λ) is evaluated using the limiting expressions:

$$J_0(x) \sim 1.0$$

$$Y_0(x) \sim \frac{2}{\pi} \left[\ln \left(\frac{1}{2} x\right) + \gamma\right] \qquad (x \text{ small})$$

$$e^{-x^2 T} \sim 1.0$$

For the profile we then obtain:

$$\int_0^{\alpha} = - \ln \rho \left\{\arctan \left[\frac{2}{\pi} \left(\ln \left(\frac{\alpha}{2}\right) + \gamma\right)\right] + \frac{\pi}{2}\right\} \tag{31}$$

with $\alpha = \min (10^{-3}, 10^{-3}/\rho, 10^{-3}/\sqrt{T})$ and for the flux:

$$\int_0^{\alpha} = \frac{\pi}{2} \left\{\arctan \left[\frac{2}{\pi} \left(\ln \left(\frac{\alpha}{2}\right) + \gamma\right)\right] + \frac{\pi}{2}\right\} \tag{32}$$

with $\alpha = \min (10^{-3}, 10^{-3}/\sqrt{T})$

The second part of the integral is evaluated using straightforward numerical integration utilizing the NAG (Numerical Algorithms Group) routine D01AGF.

For a finite cylindrical region with impermeable outer surface, r = b, boundary condition (15) is modified into.

$$\left.\frac{\partial C}{\partial r}\right|_{r=b} = 0 \tag{15a}$$

This case is of interest not only when the region is actually physically limited but also as an approximation for the case of several parallel cylindrical channels. An analytical solution of this problem is also given by Carslaw and Jaeger (1959, p. 332). The solution here is a special case of a more general solution. The solution is:

$$\frac{C}{C_o} = 1 - \pi \sum_{n=1}^{\infty} \exp\left(-\beta_n^2 T\right) J_1^2(\beta_n P)$$

$$\left[\frac{J_o(\beta_n \rho)\, Y_o(\beta_n) - Y_o(\beta_n \rho)\, J_o(\beta_n)}{J_1^2(\beta_n P) - J_o^2(\beta_n)}\right] \tag{33}$$

where β_n are the roots of

$$J_o(\beta_n)\, Y_1(\beta_n P) - Y_o(\beta_n)\, J_1^2(\beta_n P) = 0 \tag{34}$$

and P=b/a.

The flux at the surface is obtained by differentiating (33):

$$f = - D_e \left.\frac{\partial C}{\partial r}\right|_{r=a} = \frac{2D_e C_o}{a} \sum_{n=1}^{\infty} \frac{\exp(-\beta_n^2 T)\, J_1^2(\beta_n P)}{J_o^2(\beta_n) - J_1^2(\beta_n P)} \qquad (35)$$

The roots $\beta_n = \beta_n(P)$ of the nonlinear equation are determined by a Newton-Raphson iteration. Note that the roots depend on P only. Once determined, the profile may be calculated for all ρ and T and the flux for all T, for that specific value of P.

In Figure 8 the quantity $\frac{af}{D_e C_o}$ is plotted versus dimensionless time T. For the infinite region both the general solution (solid line) and the approximate ones (point-dashed lines) for small (using two terms) and large (using two terms) T are shown. It is striking how slowly the flux changes with T. Over the seven orders of magnitude shown, af/D_eC_o decreases from 6.14 at $T = 10^{-2}$ to 0.16 at $T = 10^5$. The approximation for short times is shown to be quite good for $T \leq 1.0$. The approximation for large times is good for $T \geq 10$. Note that two terms are needed in the approximations. The approximations using one term only have a much narrower range of application. Furthermore, the fluxes for the finite cylindrical shell (dashed lines) and P = 3,10,30 and 100 are also depicted in Figure 8. It is seen that the curves coincide at early times. At longer times, however, the fluxes for the finite cases fall rapidly. This occurs at specific points in time when the diffusional front reaches the outer boundary.

In Figure 9 the profiles for P = 10 (solid lines) are compared with the infinite ones (dashed lines). As expected they fully coincide at early times. At T = 10 they start to deviate somewhat near the outer

boundary and the deviation is large for T = 30. At T = 100, even for r values close to a, large deviations are seen. Obviously the flux into the matrix is now affected (lowered) as may also be seen in Figure 8.

It would be very useful to have a simple estimate of the "penetration depth" η_α^C into the cylindrical region, i.e. the location of the diffusional front. It would be a great help in numerical discretization of infinite regions to estimate to what depth discretization must be performed. As seen in Figure 8, for P = 10, the flux deviates from the flux into an infinite region when T $\geq$ 20. In Figure 9 it may be seen that the corresponding concentration at the leading edge (for the infinite diffusion) is then $C/C_0 \sim 0.05$. Also it would be very interesting to have a measure of when a finite cylindrical shell is fully equilibrated. Looking at Figure 9, $C/C_0 \sim 0.50$ (for the infinite diffusion) would be a good estimate. For a slab, calculation of the penetration depth ($C/C_0 = \alpha$; S = slab), η_α^S, is easy since:

$$\alpha = \text{erfc} \left(\frac{\eta_\alpha^S}{2\sqrt{D_a t}} \right) \tag{36}$$

giving:

$$\eta_\alpha^S = F(\alpha) \sqrt{D_a t} \tag{37}$$

For example F(0.05) = 2.77 and F(0.50) = 0.96. Such a simple solution cannot be obtained in the cylindrical case since η_α^C (C = cylinder) cannot be explicitely obtained from the profile.

Furthermore, η_α^C is also a function of the radius a. However, a useful approximation of η_α^C is the following. As seen in Figure 9 or in Carslaw and Jaeger (1959, p. 337) the concentration profiles when plotted in a lin-log diagram are nearly linear except for small C/C_o. The equation for a straight line cutting the C/C_o-axis at $C/C_o = 1.0$ and with slope given by the slope at the same point is:

$$C/C_o = - \frac{af}{C_o D_e} \ln 10 \log \left(\frac{r}{a}\right) + 1.0 \tag{38}$$

where f is the flux at the interface r = a. The approximation is shown for T = 0.1 in Figure 9 (dashed-dot line).

A good approximation of the leading edge (η_e^C) is obtained by taking the point where the straight line cuts the log $(\frac{r}{a})$-axis ($C/C_o = 0.0$). We obtain:

$$\log \left(\frac{\eta_e^C}{a}\right) = \frac{1.0}{\frac{af}{C_o D_e} \ln 10} \tag{39}$$

The point obtained is not exactly $C/C_o = 0.05$ but somewhat higher at early times and decreasing with time. In a similar fashion a very good approximation of $\eta_{0.50}^C$ is:

$$\log \left(\frac{\eta_{0.50}^C}{a}\right) = \frac{0.5}{\frac{af}{C_o D_e} \ln 10} \tag{40}$$

Explicit expressions for η^C for $T \leq 1.0$ and $T \geq 10.0$ may be obtained using the limiting expressions given in Table 1 (with two terms). In the intermediate range the value of $\frac{af}{C_o D_e}$ may be read from Figure 8.

Comparison cylinder and slit

It is of interest to compare diffusion from cylindrical and slit-formed channels. Choosing the same interfacial area we would expect that the uptake should be the same at short times since only the surface region is affected. For larger penetration the concentration profiles, from the slit, are governed by the length/breadth ratio of the slit source. However, for large penetration, the uneven concentration distribution is smoothed and approximately resembles the one from a cylindrical source. Comparing fluxes from slits of various length/breadth ratios with the cylindrical source we would therefore expect deviations at intermediate times only.

Calculations, for the slit, were made with the computer program TRUMP (Edwards, 1972). A mesh generator was written to define the subvolumes and their interconnections. Calculations were made with the interfacial area $\pi \cdot 10^{-2}$ m^2/m corresponding to a cylindrical tube with diameter 10^{-2} m. The diffusivity, $D_p \varepsilon_p$, is $5 \cdot 10^{-14}$ m^2/s and $K = 1.0$. The length/breadth ratios were 1.0, 2.0, 4.0, 16.0 and infinity. In Figure 10 the fluxes f in mol/m^2, yr are plotted versus time (in years). The concentration C_o at the surface is set to 1 mol/m^3. It is seen that the differences are surprisingly small.

FLOW IN CYLINDRICAL CHANNELS

Analytical solutions

Van Genuchten et al (1984) present exact and approximate solutions of equations (1) and (2) subject to boundary conditions (7) - (12) (without radioactive decay). They were concerned with the problem of solute transport through soils containing large cylindrical macropores.

The exact solutions for the concentration distribution in the macropores are obtained following methods similar to those used by Rasmuson and Neretnieks (1980). The solutions have the same structure as the solution derived by Rasmuson and Neretnieks for advective-dispersive transport between spherical particles. It is:

$$C_f/C_o = \frac{1}{2} + \frac{2}{\pi} \int_0^\infty \exp\left[-g(p_i,\lambda)\right] \sin\left[h(p_i,y,\lambda)\right] \frac{d\lambda}{\lambda} \qquad (41)$$

where p_i are various dimensionless parameters, y is a dimensionless time and g and h are complicated groups of Bessel functions.

When longitudinal dispersion in the cylindrical fracture is neglected ($D_L \rightarrow 0$) and the matrix is infinite van Genuchten et al (1984) obtained the following approximate solution valid for small values of time:

$$C_f/C_o = \exp\left[\frac{-D_p\varepsilon_p z}{a^2 V}\right] \operatorname{erfc}\left[\frac{D_p\varepsilon_p z}{aV} \frac{1}{\left[\frac{D_p\varepsilon_p}{K}\left(t - \frac{R_a z}{V}\right)\right]^{1/2}}\right] \qquad (42)$$

Apart from the exponential factor this solution is identical to the solution for the concentration distribution in a planar fracture with infinite matrix (Neretnieks, 1980). This is to be expected since for short contact times the uptake in planar and cylindrical walls are the same.

Numerical scheme

The IFDM scheme used in this paper was originally developed by Edwards (1972) who incorporated it into a computer program called TRUMP. The method, as applied to chemical transport, is fully described by Rasmuson et al (1982). To facilitate the computations a mesh generator for the present case was written. The generator gives an output-file of the same format as the original input to TRUMP.

The program was tested against the analytical result given by van Genuchten et al (1984) (their Figure 2) with excellent agreement.

Results and discussion

The data used in the numerical calculations are given in Table 2. The calculations are done for Np-237. The density of cylindrical tubes is assumed to be one tube/m^2 cross-sectional area. This is based on the experimental observations in the Swedish KBS-3 study (KBS, 1983). In the bore-holes it was found that, on the average, the fracture spacing is 1 m. However, only every fifth fracture carried any water. The assumption taken here is that all fractures transport water but only in channels in the fracture plane.

The experimental observation could then be explained by the channel distribution as depicted in Figure 6. Each channel is here 0.2 m wide separated by impermeable zones 1 m wide.

As the geometrical shape of the channel seems to be of minor importance (compare with Figure 10) we approximate the flat channel with interfacial area 0.4 m^2/m with a cylindrical channel with the same contact area giving a = $6.3662 \cdot 10^{-2}$ m. Diffusional transport in the matrix is then treated as 1-D instead of 2-D which gives a considerable numerical simplification. The value a = $5.0 \cdot 10^{-3}$ m is taken as an extreme case. In this case the interfacial area is $3.14 \cdot 10^{-2}$ m^2/m only.

The fairly high Peclet numbers chosen reflect the fact that we treat a set of parallel individual channels with no interconnections. Hydrodynamic dispersion is then mainly caused by a distribution of flow rates and retention times between the different channels (Neretnieks, 1983; Rasmuson, 1985). Ideally, therefore each channel should be treated with little or no dispersion. However, there are inherent difficulties in numerical schemes at high Peclet numbers. In the case of no matrix diffusion, Rasmuson et al (1982) showed that stable solutions are obtained if the local numerical Peclet number is less than two:

$$Pe_{\ell} = \frac{\Delta z V}{2 D_L} < 2$$

giving:

$$\frac{\Delta z}{L} < \frac{4}{Pe} \tag{43}$$

The accuracy is increased with decreasing Pe_ℓ. In our example, where L = 100, we obtain $\Delta z < 40$ m (Pe = 10) and $\Delta z < 8$ m (Pe = 50). In the calculations Δz varied between 2 and 4 m which should be sufficient for an accurate solution.

The values of the flow rate are typical for undisturbed rock (Q = 0.1 $\ell/m^2,yr$) and a crushed zone (Q = 1.0 $\ell/m^2,yr$) respectively. The value for undisturbed rock is based on the Swedish KBS-3 study (KBS, 1983). The flow rate in the crushed zone is assumed to be higher due to higher hydraulic conductivity (Neretnieks and Rasmuson, 1984). Finally the values of the volume equilibrium constant, K, and the effective diffusivity, $D_p\varepsilon_p$, are as given in the KBS-3 study (KBS, 1983).

The matrix is treated as infinite in the computations. The diffusional fronts will not meet until r = 0.5 m. Using the half-life as a characteristic time we obtain $T = 6.16 \cdot 10^{-2}$ ($a = 6.3662 \cdot 10^{-2}$ m) and T = 9.99 ($a = 5.0 \cdot 10^{-3}$ m). Comparing with Figure 9 it may be seen that the penetration depth is indeed considerably less than 0.5 m.

The results for Q = 0.1 $\ell/m^2,yr$ ("undisturbed rock") and Pe = 10 are depicted in Figure 11 and for Q = 1.0 $\ell/m^2,yr$ ("crushed zone") and Pe = 10 in Figure 12. For comparison the breakthrough curves with surface retardation only are also shown as well as a calculation where

the rock is assumed to consist of a cubic system of orthogonal fractures. The surface retardation coefficient is obtained from:

$$R_a = \left[\left(1 + \frac{\eta}{a}\right)^2 - 1\right] K + 1 \qquad (44)$$

where η is the penetration depth. Under the assumption that η = 0.1 mm, that is 0.1 mm of the rock adjacent to the channel is instantaneously equilibrated, we get $R_a = 5.4640 \cdot 10^2$ ($a = 5.0 \cdot 10^{-3}$ m) and $R_a = 4.3445 \cdot 10^1$ ($a = 6.3662 \cdot 10^{-2}$ m). The cubical blocks are approximated by spheres having the same area-to-volume ratio. Assuming S = 5 m gives r_o = 2.5 m. The interfacial area is 1.2 m^2/m^3. The Peclet number is 2 in these calculations indicating a system with large hydrodynamic dispersion.

It may be seen that matrix diffusion from the cylindrical channel has a large impact on the breakthrough curve. If surface retardation only is in effect the breakthrough is delayed but no significant reduction in effluent concentration is obtained. In the case of matrix diffusion the negative effect of a small surface area is substantially compensated for by diffusion into the cylindrical matrix and the peak-heights are much lower. Note again that for the case of spherical blocks Pe = 2. For Pe = 10 the peak-heights are much lower, $< 10^{-11}$ (Q = 0.1 ℓ/m^2,yr) and $6 \cdot 10^{-4}$ (Q = 1.0 ℓ/m^2,yr).

Comparing Figure 11 and Figure 12 it is seen that the flow rate has a large impact. The breakthrough occurs much earlier for Q = 1.0 ℓ/m^2,yr.

Finally, in Figures 13 and 14 the influence of the Peclet-number, for the cases of flow and diffusion into the cylindrical matrix is given. It is seen that the Peclet number has a strong influence on the early arrival of the nuclide. Less dispersion in these cases produce lower peak heights because the breakthrough occurs later giving more time for the radionuclide to decay.

CONCLUSIONS

When the water flow takes place in individual small channels in fractures the surface in direct contact with water is smaller than if the whole fracture surface was wetted. This has consequences for the retardation of sorbing species. When the sorption takes place on the channel surfaces only, the retardation in some studied cases may be very small compared to when the rock matrix is porous. In the latter case the species diffuse into the matrix and contact an increasing volume of rock as the distance from the channel increases. If the penetrated distance is larger than the largest dimension of the channel (not counting the flow direction) the geometry of the channel has little importance and can be approximated by a cylinder with the same circumference. This simplifies the computations considerably.

The theoretical analysis has shown very clearly that in general channel geometry and the frequency of channels have a very strong impact on the transport of dissolved species. Such data are largely not available. Dispersion in individual channels as well as in networks of channels has a strong impact. Dispersion data and information on channel intersections and transport in such networks is not available. We feel that the growing experimental evidence that channeling is more a rule than an exception might warrant further work in this direction.

NOTATION

a	radius of cylindrical channel	L
b	outer radius of cylindrical mantle in case of finite matrix	L
C	concentration in water	M/L^3
C_f	concentration in water in fissures	M/L^3
C_p	concentration in water in microfissures	M/L^3
C_o	inlet concentration in the water	M/L^3
D_a	$= \frac{D_p \varepsilon_p}{K}$, apparent diffusivity in micro-fissures	L^2/T
D_e	$= D_p \varepsilon_p$, effective diffusivity in micro-fissures	L^2/T
D_{eo}	effective diffusivity at the surface x=0	L^2/T
D_L	longitudinal dispersion coefficient	L^2/T
D_p	diffusivity in water in pores	L^2/T
D_v	diffusivity in water	L^2/T
f	molar flux from flowing water to rock matrix	$M/L^2,T$
J_o, J_1	Bessel function of first kind of order zero and one	
K	volume equilibrium constant	
K_a	sorption equilibrium constant	
K_f	surface distribution coefficient	L
P	$= b/a$	
Pe	$= \frac{zV}{D_L}$, Peclet number	

Q	water flow rate	$L^3/L^2,T$
R_a	$= 1 + \beta K_f$, surface retardation coefficient	
r	radial coordinate	L
r_o	effective spherical radius	L
S	fissure spacing	L
T	$= \frac{D_a t}{a^2}$, dimensionless time	
$T_{1/2}$	half-life	T
t	time	T
V	average velocity of water in fissures	L/T
x	distance into slab	L
Y_o, Y_1	Bessel function of second kind of order zero and one	
z	distance in flow direction	L

Greek letters

β	interfacial rock surface per unit fracture volume	L^2/L^3
δ_D	constrictivity for diffusion	
ε_f	porosity of fissures	
ε_p	porosity of rock matrix	
η	penetration depth	L
κ	parameter in equation (27)	
λ	decay constant of radionuclide	T^{-1}
ρ	$= r/a$, dimensionless radius	
τ	tortuosity	

ACKNOWLEDGMENTS

This work was supported by the Swedish Nuclear Fuel Supply Company.

REFERENCES

Abelin, H., I. Neretnieks, S. Tunbrant and L. Moreno: Migration in a single fracture. Experimental results and evaluation. Final report, Stripa project, May 1985.

Carslaw, H.S. and J.C. Jaeger: Conduction of Heat in Solids, 2nd ed., Oxford at the Clarendon Press, London, 1959.

Edwards, A.L.: TRUMP: A computer program for transient and steady state temperature distributions in multidimensional systems. National Technical Information Service, National Bureau of Standards, Springfield Va., 1972.

KBS-Nuclear Fuel Safety Project. Final storage of spent nuclear fuel, Tech. Rep. KBS-3, Stockholm, 1983.

NAGRA-Nationale Genossenschaft für die Lagerung radioaktiver Abfälle, Projektbericht NGB 85-04, 1985.

Neretnieks, I.: Diffusion in the rock matrix: An important factor in radionuclide retardation? J. Geophys. Res. 85, 4379-4397, 1980.

Neretnieks, I.: A note on fracture flow dispersion mechanisms in the ground. Water Resour. Res. 19, 364-370, 1983.

Neretnieks, I.: Transport in fractured rock. Paper presented at the IAH 17th International Congress on the Hydrology of Rocks of Low Permeability, Tucson, Arizona, Jan. 1985, proceedings in print.

Neretnieks, I. and A. Rasmuson: An approach to modelling radionuclide migration in a medium with strongly varying velocity and block sizes along the flow path. Water Resour. Res. 20, 1823-1836, 1984.

Rasmuson, A.: Analysis of hydrodynamic dispersion in discrete fracture networks using the method of moments. Water Resour. Res. 21, 1677-1683, 1985.

Rasmuson, A. and I. Neretnieks: Exact solution of a model for diffusion in particles and longitudinal dispersion in packed beds, AIChE J. 26, 686-690, 1980.

Rasmuson, A., T.N. Narasimhan and I. Neretnieks: Chemical transport in a fissured rock: Verification of a numerical model. Water Resour. Res. 18, 1479-1492, 1982.

Skagius, K.: Personal communication, 1985.

van Genuchten, M.T., D.H. Tang and R. Guennelon: Some exact solutions for solute transport through soils containing large cylindrical macropores. Water Resour. Res. 20, 335-346, 1984.

Interval	Profile $(\frac{C}{C_o})$	Flux$\Big\vert_{r=a}$ (f)
$0 \leq T \leq \infty$	$1 + \frac{2}{\pi} \int_0^\infty e^{-\lambda^2 T} \frac{J_o(\lambda\rho)\, Y_o(\lambda) - Y_o(\lambda\rho)\, J_o(\lambda)}{J_o^2(\lambda) + Y_o^2(\lambda)} \frac{d\lambda}{\lambda}$ (17)	$\frac{4C_o D_e}{a\pi^2} \int_0^\infty e^{-\lambda^2 T} \frac{d\lambda}{\lambda[J_o^2(\lambda) + Y_o^2(\lambda)]}$ (20)
small T	$\frac{1}{\sqrt{\rho}} \operatorname{erfc}\left(\frac{\rho-1}{2\sqrt{T}}\right) + \left(\frac{1}{\sqrt{\rho}} - \frac{1}{\rho\sqrt{\rho}}\right) \frac{\sqrt{T}}{4} \operatorname{ierfc}\left(\frac{\rho-1}{2\sqrt{T}}\right) + \ldots$ (18)	$\frac{C_o D_e}{a} \left(\frac{1}{\sqrt{\pi T}} + \frac{1}{2} - \frac{1}{4}\sqrt{\frac{T}{\pi}} + \frac{1}{8} T - \ldots\right.$ (21)
large T (ρ not too large)	$1 + 2 \ln \rho \left[- \frac{1.0}{\ln(4T) - 2\gamma} + \frac{\gamma}{(\ln(4T) - 2\gamma)^2} \right.$ (19)	$\frac{2C_o D_e}{a} \left[\frac{1}{\ln(4T) - 2\gamma} - \frac{\gamma}{(\ln(4T) - 2\gamma)^2}\right.$ (22)
	$\left. + \frac{\frac{\pi^2}{6} - \gamma^2}{(\ln(4T) - 2\gamma)^3} + \ldots \right.$	$\left. - \ldots \right.$

Table 1. Diffusion in an infinite region bounded internally by the circular cylinder r=a. General analytical expressions (Carslaw and Jaeger, 1959) for profile and flux at the surface as well as limiting expressions for small and large values of T. $\rho = r/a$, $T = D_a t/a^2$ and γ = Euler's const. = 0.57722.

Parameter	Dimension	Value
Travel distance, L	m	100
Tube radius, a	m	$5.0 \cdot 10^{-3}$ and $6.3662 \cdot 10^{-2}$
Volumetric flow rate, Q	$\ell/m^2,yr$ (ℓ/tube,yr)	0.1 and 1.0
Peclet number, Pe	-	10 and 50
Surface retardation coefficient, R_a	-	1.0
Volume equilibrium constant, K	m^3/m^3	$1.35 \cdot 10^4$
Effective diffusivity in rock matrix, $D_p\varepsilon_p$	m^2/s	$5.0 \cdot 10^{-14}$
Half-life of Np-237, $T_{1/2}$	years	$2.14 \cdot 10^6$

Table 2. Data used in numerical calculations of flow in cylindrical tubes with matrix diffusion.

FIGURES

Figure 1 Correlation between hydraulic conductivity and depth for the rock mass at Kamlunge.

Figure 2 Total fracture frequency and hydraulic fracture frequency (shaded) in the rock mass within the sites at Finnsjön (left-hand figure) and Sternö (right-hand figure).

Figure 3 Average water flow rate from fracture 1 and fracture 2 in Stripa.

Figure 4 Water flow rate into 3-D drift at Stripa before drilling the injection holes.

Figure 5 Channels with mobile water within a fracture plane are formed between the areas of contact of the surfaces.

Figure 6 Fractures within a large block of rock are intersected by the exploratory borehole. The hole intersects five fractures but only one channel conducts water.

Figure 7 Flux, f, at the surface of regions bounded internally by a circular cylinder or sphere of radius a and semi-infinite slab, with zero initial concentration and constant surface concentration C_o.

Figure 8 Flux, f, at the surface of the region bounded internally by a circular cylinder of radius a. Infinite and finite matrix.

Figure 9 Concentration profiles into infinite (dashed lines) and finite (solid lines) matrix with P = 10.

Figure 10 Flux, f, at the surface of the region bounded internally by a cylinder and by slits with various length/breadth ratios. The interfacial area is in all cases $\pi \cdot 10^{-2}$ m^2/m.

Figure 11 Breakthrough curves at the distance 100 m in cylindrical fractures with radius a = $5 \cdot 10^{-3}$ and $6.3662 \cdot 10^{-2}$ m and matrix diffusion (dashed lines) and surface retardation (solid lines). Q = 0.1 $\ell/m^2,yr$ and Pe = 10.

Figure 12 Same as Figure 11 but Q = 1.0 $\ell/m^2,yr$.

Figure 13: Breakthrough curves at the distance 100 m in cylindrical fractures with radius a = $5 \cdot 10^{-3}$ and $6.3662 \cdot 10^{-2}$ m and matrix diffusion. Influence of Peclet number. Q = 0.1 $\ell/m^2,yr$.

Figure 14 Same as Figure 13 but Q = 1.0 $\ell/m^2,yr$.

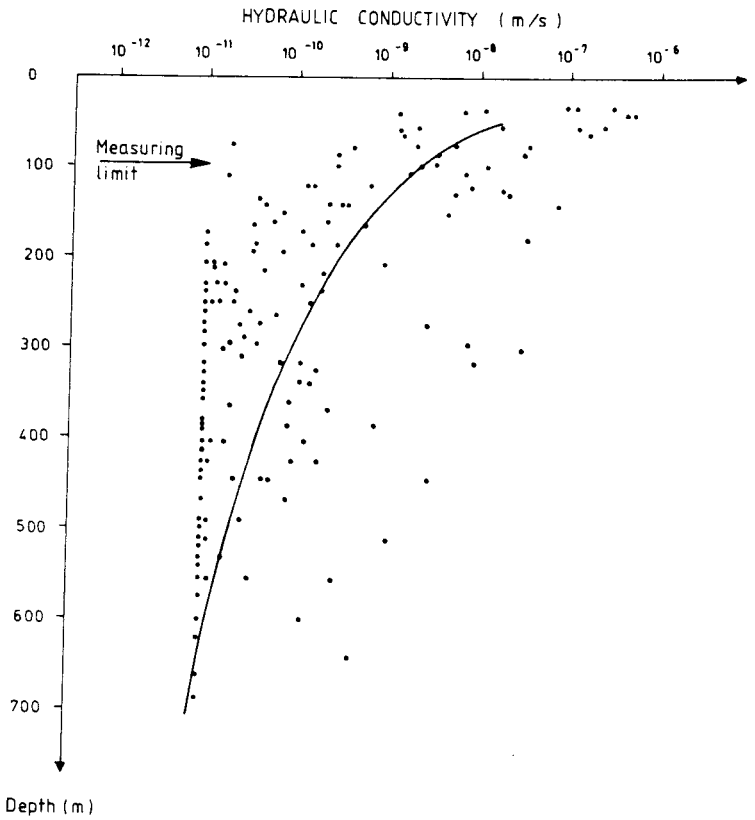

Figure 1.

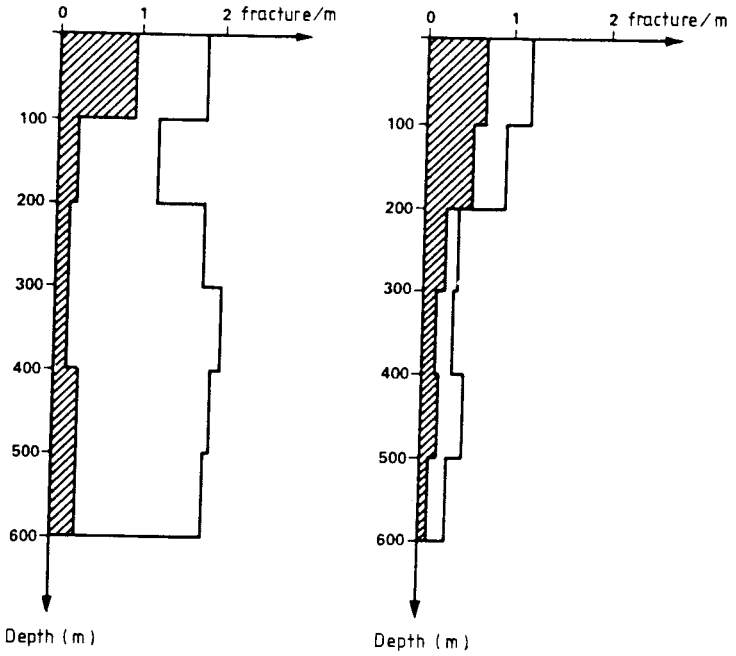

Figure 2.

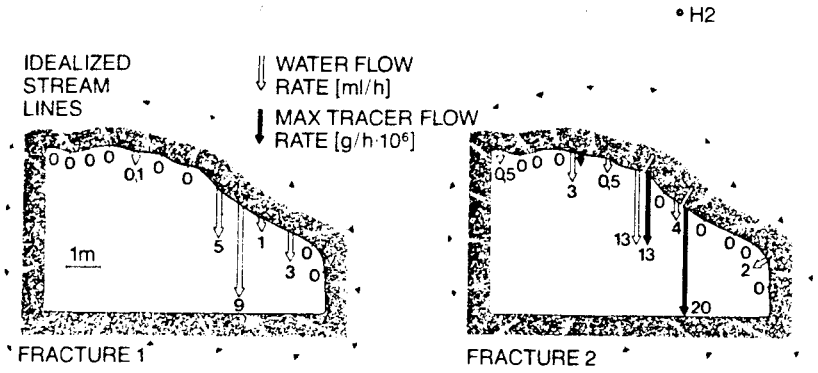

Figure 3.

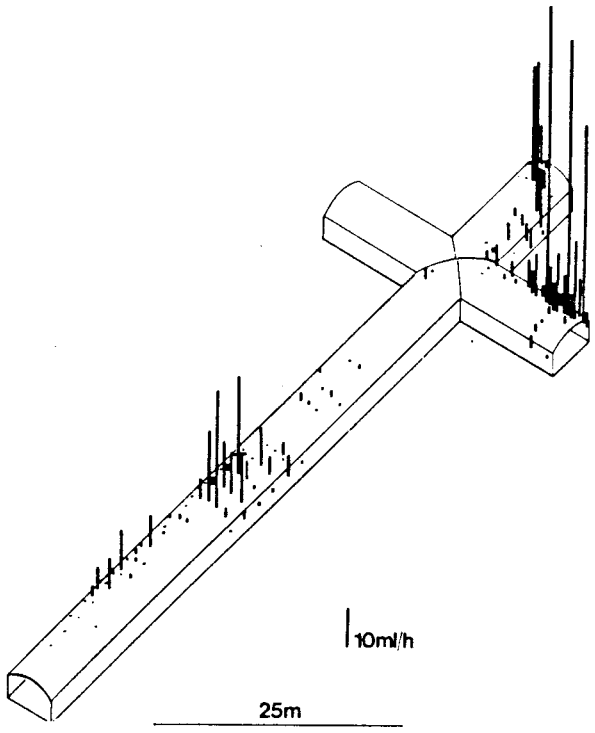

Figure 4.

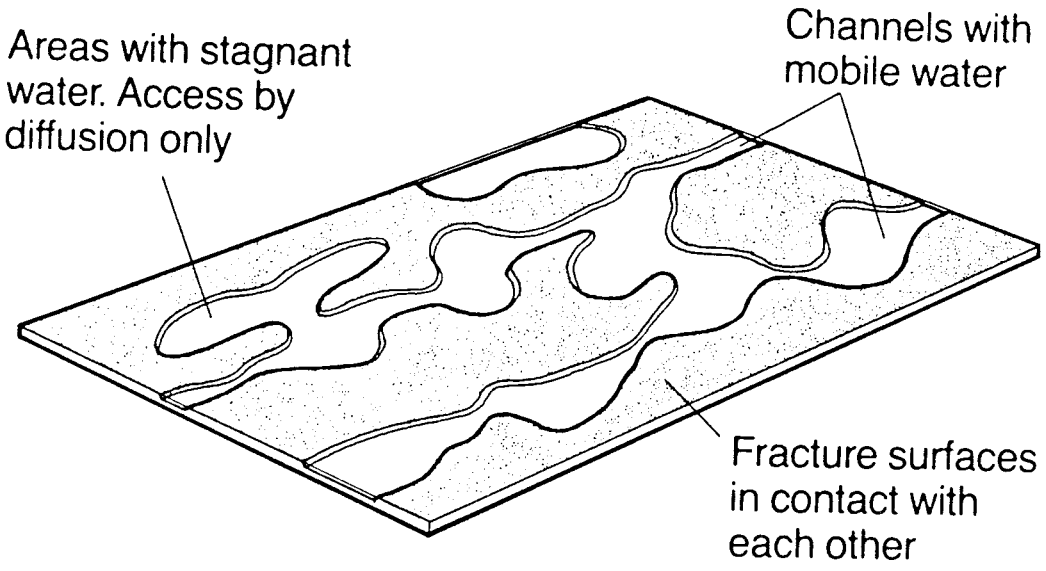
Areas with stagnant water. Access by diffusion only
Channels with mobile water
Fracture surfaces in contact with each other

Figure 5.

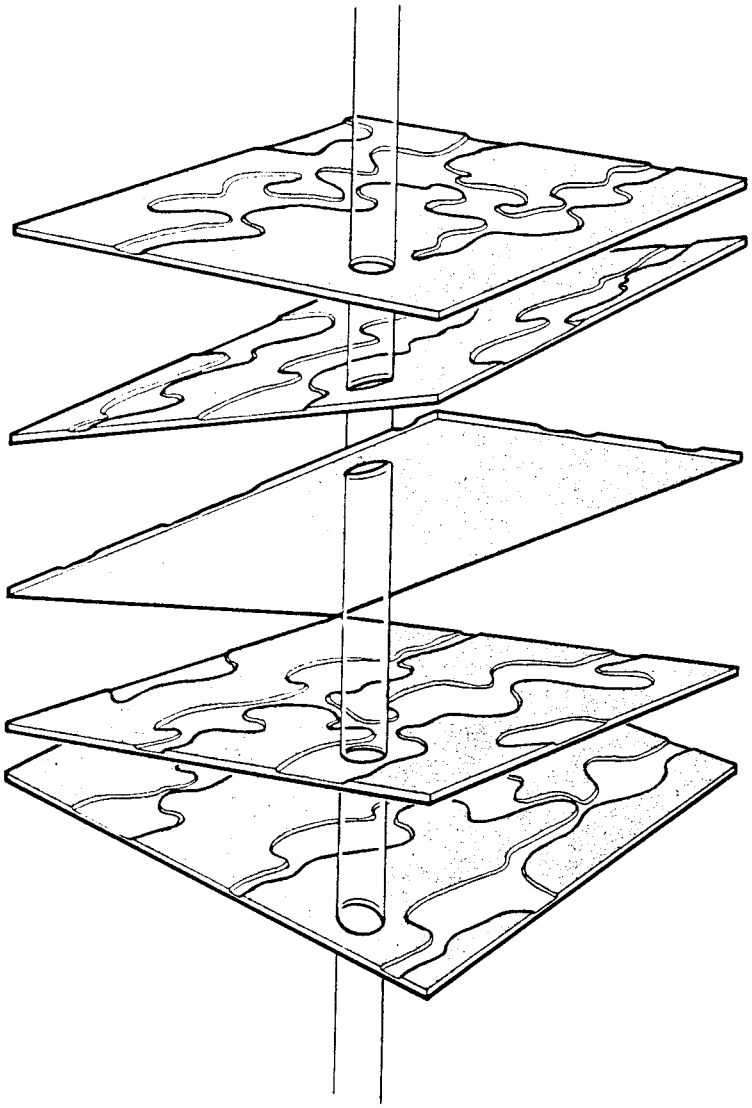

Figure 6.

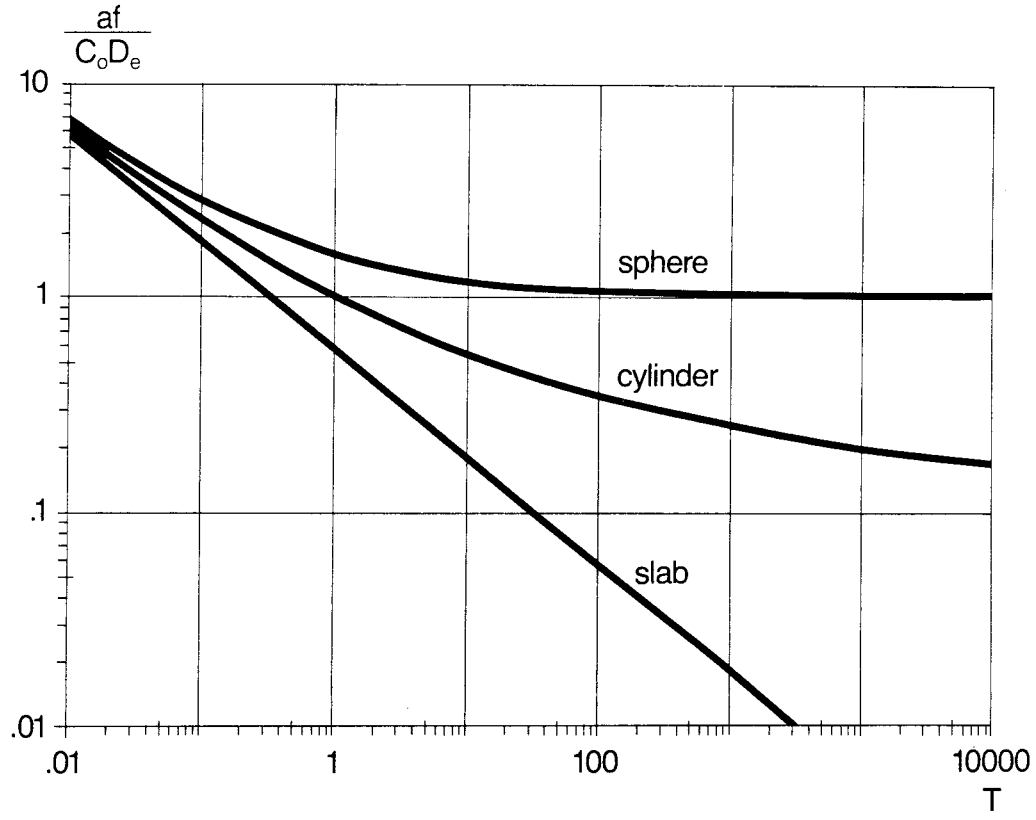

Figure 7.

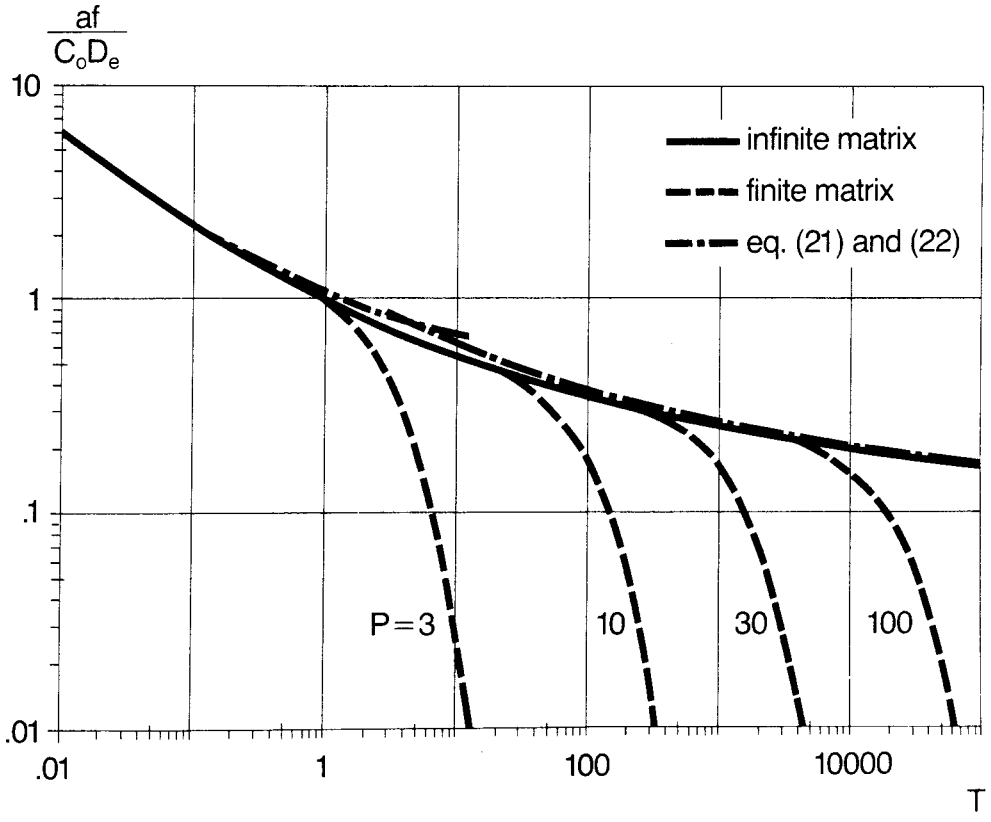

Figure 8.

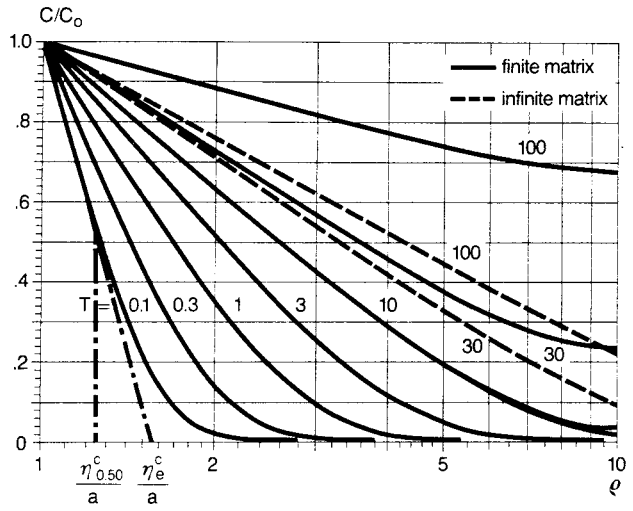

Figure 9.

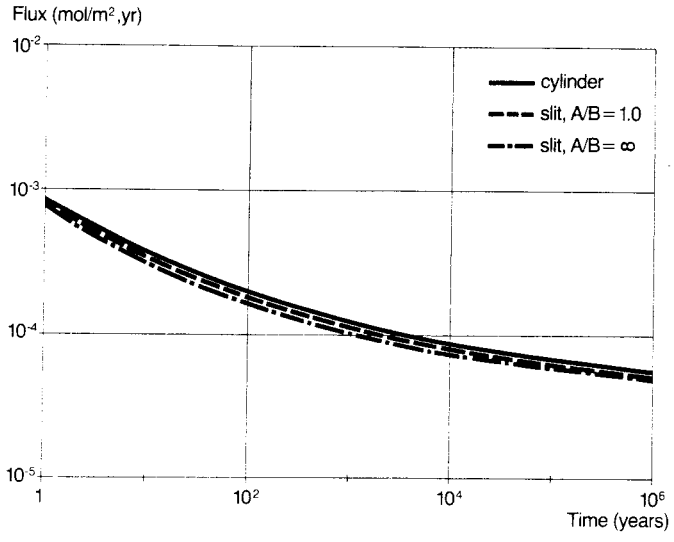

Figure 10.

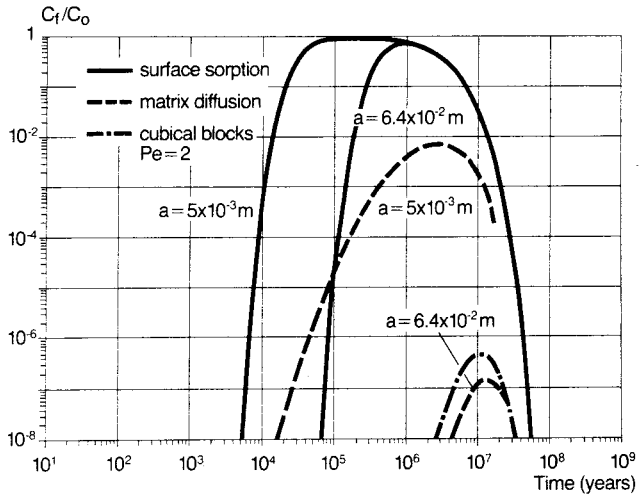

Figure 11.

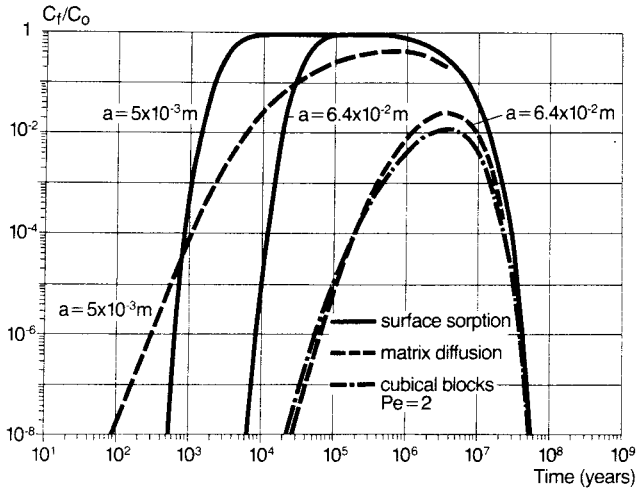

Figure 12.

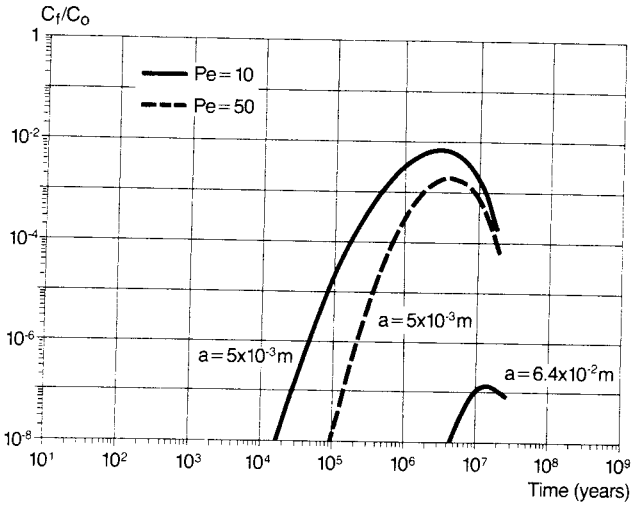

Figure 13.

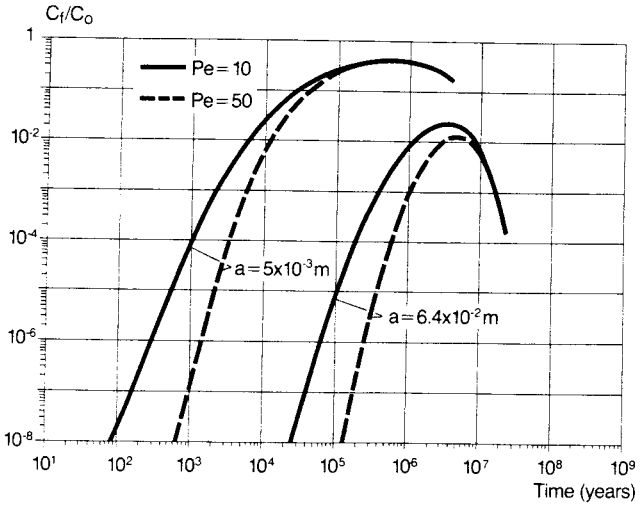

Figure 14.

List of SKB reports

Annual Reports

1977–78
TR 121
KBS Technical Reports 1 – 120.
Summaries. Stockholm, May 1979.

1979
TR 79–28
The KBS Annual Report 1979.
KBS Technical Reports 79-01 – 79-27.
Summaries. Stockholm, March 1980.

1980
TR 80–26
The KBS Annual Report 1980.
KBS Technical Reports 80-01 – 80-25.
Summaries. Stockholm, March 1981.

1981
TR 81–17
The KBS Annual Report 1981.
KBS Technical Reports 81-01 – 81-16.
Summaries. Stockholm, April 1982.

1982
TR 82–28
The KBS Annual Report 1982.
KBS Technical Reports 82-01 – 82-27.
Summaries. Stockholm, July 1983.

1983
TR 83–77
The KBS Annual Report 1983.
KBS Technical Reports 83-01 – 83-76
Summaries. Stockholm, June 1984.

1984
TR 85–01
Annual Research and Development Report 1984
Including Summaries of Technical Reports Issued during 1984. (Technical Reports 84-01– 84-19)
Stockholm June 1985.

1985
TR 85-20
Annual Research and Development Report 1985
Including Summaries of Technical Reports Issued during 1985. (Technical Reports 85-01-85-19)
Stockholm May 1986.

Technical Reports

1986

TR 86-01
I: An analogue validation study of natural radionuclide migration in crystalline rock using uranium-series disequilibrium studies
II: A comparison of neutron activation and alpha spectroscopy analyses of thorium in crystalline rocks
J A T Smellie, Swedish Geological Co, A B MacKenzie and R D Scott, Scottish Universities Research Reactor Centre
February 1986

TR 86-02
Formation and transport of americium pseudocolloids in aqueous systems
U Olofsson
Chalmers University of Technology, Gothenburg, Sweden
B Allard
University of Linköping, Sweden
March 26, 1986

TR 86-03
Redox chemistry of deep groundwaters in Sweden
D Kirk Nordstrom
US Geological Survey, Menlo Park, USA
Ignasi Puigdomenech
Royal Institute of Technology, Stockholm, Sweden
April 1, 1986

TR 86-04
Hydrogen production in alpha-irradiated bentonite
Trygve Eriksen
Royal Institute of Technology, Stockholm, Sweden
Hilbert Christensen
Studsvik Energiteknik AB, Nyköping, Sweden
Erling Bjergbakke
Risö National Laboratory, Roskilde, Denmark
March 1986

TR 86-05
Preliminary investigations of fracture zones in the Brändan area, Finnsjön study site
Kaj Ahlbom, Peter Andersson, Lennart Ekman, Erik Gustafsson, John Smellie,
Swedish Geological Co, Uppsala
Eva-Lena Tullborg, Swedish Geological Co, Göteborg
February 1986

TR 86-06
Geological and tectonical description of the Klipperås study site
Andrzej Olkiewicz
Vladislav Stejskal
Swedish Geological Company
Uppsala, June 1986

TR 86-07
Geophysical investigations at the Klipperås study site
Stefan Sehlstedt
Leif Stenberg
Swedish Geological Company
Luleå, July 1986

TR 86-08
Hydrogeological investigations at the Klipperås study site
Bengt Gentzschein
Swedish Geological Company
Uppsala, June 1986

TR 86-09
Geophysical laboratory investigations on core samples from the Klipperås study site
Leif Stenberg
Swedish Geological Company
Luleå, July 1986

TR 86-10
Fissure fillings from the Klipperås study site
Eva-Lena Tullborg
Swedish Geological Company
Göteborg, June 1986

TR 86-11
Hydraulic fracturing rock stress measurements in borehole Gi-1, Gideå Study Site, Sweden
Bjarni Bjarnason and Ove Stephansson
Division of Rock Mechanics,
Luleå University of Technology, Sweden
April 1986

TR 86-12
PLAN 86—Cost for management of the radioactive waste from nuclear power production
June 1986